Coordination of operational planning and real-time optimization in microgrids

Jonathan Dumas*, Selmane Dakir*, Clément Liu†, Bertrand Cornélusse*
*Department of electrical engineering and computer science
ULiège, Liège, Belgium
{jdumas, s.dakir, bertrand.cornelusse}@uliege.be
†clement.liu@polytechnique.edu

***Abstract*—Hierarchical microgrid control levels range from distributed device level controllers that run at a high frequency to centralized controllers optimizing market integration that run much less frequently. Centralized controllers are often subdivided into operational planning controllers that optimize decisions over a time horizon of one or several days, and real-time optimization controllers that deal with actions in the current market period. The coordination of these levels is of paramount importance. In this paper, we propose a value function-based approach as a way to propagate information from operational planning to real-time optimization. We apply this method to an environment where operational planning, using day-ahead forecasts, optimizes at a market period resolution the decisions to minimize the total energy cost and revenues, the peak consumption and injection-related costs, and plans for reserve requirements. While real-time optimization copes with the forecast errors and yields implementable actions based on real-time measurements. The approach is compared to a rule-based controller on three use cases, and its sensitivity to forecast error is assessed.**

***Index Terms*—Hierarchical control, microgrid, optimization**

I. Introduction

The hierarchical microgrid control levels divide a global microgrid control problem in time and space [1]. Control levels range from distributed device level controllers that run at a high frequency to centralized controllers optimizing market integration that run much less frequently. For computation time reasons, centralized controllers are often subdivided into operational planning controllers that optimize decisions over a time horizon of one or several days but with a market period resolution, *e.g.*, 15 minutes, and real-time optimization controllers that deal with actions within the current market period. The coordination of these two levels is of paramount importance to achieve the safest and most profitable operational management of microgrids. Microgrid control and management can be achieved in several ways. Control techniques and the principles of energy-storage systems are summarized in [1]. A classification of microgrid control strategies into primary, secondary, and tertiary levels is done in [2]. The two-level approach has been intensively studied. A double-layer coordinated control approach, consisting of the schedule layer and the dispatch layer is adopted in [3]. The schedule layer provides an economical operation scheme including state and power of controllable units based on the look-ahead multi-step optimization, while the dispatch layer follows the schedule layer by considering power flow and voltage limits. A two-stage dispatch strategy for grid-connected systems is discussed in [4], where the first stage deals with the day-ahead schedule, optimizing capital and operational cost, while the lower level handles the rescheduling of the units for few hours ahead with a time resolution of 15 min. A two-stage control strategy for a PV BESS-ICE (Internal Combustion Engine) microgrid is implemented in [5]. Discrete Dynamic Programming is used in the first layer, while the second layer problem is posed as a Boundary Value Problem. An approach with a high-level deterministic optimizer running at a slow timescale, 15 min, coupled to a low-level stochastic controller running at higher frequency, 1 min, is studied in [6]. A two-layer predictive energy management system for microgrids with hybrid energy storage systems consisting of batteries and supercapacitors is considered in [7]. This approach incorporates the degradation costs of the hybrid energy storage systems. A practical Energy Management System for isolated microgrid which considers the operational constraints of Distributed Energy Resources, active-reactive power balance, unbalanced system configuration and loading, and voltage-dependent loads is studied in [8]. A two-layer mixed-integer linear programming predictive control strategy was implemented and tested in simulation and experimentally in [9], and [10] implemented a two-layer predictive management strategy for an off-grid hybrid microgrid featuring controllable and non-controllable generation units and a storage system.

In this paper, we propose a two-layer approach with a value function to propagate information from operational planning to real-time optimization. The value function-based approach shares some similarities with the coordination scheme proposed in [11], which is based on stochastic dual dynamic programming. This paper brings new contributions:

- The approach is tested by accounting for forecasting errors and high-resolution data monitored on-site corresponding to a "real-life" case.
- The value function approach allows to deal with indeterminacy issues. When there are several optimal solutions to the upper-level problem, this is accounted for in the lower level part, and a bias term can be added to favor one type of behavior over another, *e.g.*, charge early.
- This methodology is fully compatible with the energy

markets as it can deal with imbalance, reserve, and dynamic selling/purchasing prices.

This paper reports results on an industrial microgrid capable of on/off grid operation. Generation and consumption forecasts are based on weather forecasts obtained with the MAR model [12]. It is organized as follows. Section II formulates the problem in an abstract manner. Section III introduces the novel two-level value function-based approach and the assumptions made. Section IV describes the numerical tests. Section V reports the results. Conclusions are drawn in Section VI. Section VIII summarizes the notation. The methodology used for forecasting is reported as an annex.

II. Problem statement

A global microgrid control problem can be defined, for a given microgrid design and configuration, as operating a microgrid safely and in an economically efficient manner, by harvesting as much renewable energy as possible, operating the grid efficiently, optimizing the service to the demand side, and optimizing other side goals. We refine this definition below and start by making a few assumptions.

A. Assumptions

In this paper, the control optimizes economical criteria, which are only related to active power. All devices are supposed to be connected to the same electrical bus, which can be connected or disconnected from a public grid permanently or dynamically. Device-level controllers offer an interface to communicate their operating point and constraints, *e.g.*, maximum charge power as a function of the current state, and implement control decisions to reach power set-points. Fast load-frequency control, islanding management, as well as reactive power control, are not in scope. The microgrid is a price taker in energy and reserve markets.

B. Formulation

Abstractly, a microgrid optimization problem can be formulated as follows

$$\min_{\mathbf{a}} \quad \sum_{t\in\mathcal{T}_l} c(a_t, s_t, \omega_t) \tag{1a}$$

$$\text{s.t. } \forall t \in \mathcal{T}_l,\ s_{t+\Delta t} = f(a_t, s_t, \omega_t, \Delta t), \tag{1b}$$

$$s_t \in \mathcal{S}_t. \tag{1c}$$

A controller has to return a set of actions $a_t = (a_t^m, a_t^d)$ at any time t over the life of the microgrid ($\mathcal{T}_l$). Actions should be taken as frequently as possible to cope with the economic impact of the variability of the demand and generation sides, but not too often to let transients vanish, *e.g.*, every few seconds. The time delta between action a_t and the next action taken is denoted by Δ_t, and is not necessarily constant. Some of these actions are purely market-related a_t^m, while other actions are communicated as set-points to the devices of the microgrid a_t^d. The state $s_t = (s_t^m, s_t^d)$ of the microgrid at time t is thus also made of two parts: s_t^d represents the state of the devices, such as the state of charge of a storage system or the state of a flexible load, while s_t^m gathers information related to the current market position, such as the nominated net position of the microgrid over the next market periods. The cost function c gathers all the economical criteria considered. The transition function f describes the physical and net position evolution of the system. At time instants $t \in \{\Delta_\tau, 2\Delta_\tau, \dots\}$, with Δ_τ the market period, some costs are incurred based on the value of some state variables, which are then reset for the next market period. This problem is very difficult to solve since the evolution of the system is uncertain, actions have long-term consequences, and are both discrete and continuous. Furthermore, although functions f and c are assumed time-invariant, they are generally non-convex and parameterized with stochastic variables ω_t.

III. Proposed method

In practice, solving the microgrid optimization problem above amounts, at every time t, to forecasting the stochastic variables $\boldsymbol{\omega}_{\mathcal{T}_l(t)}$, then solving the problem[1]

$$\mathbf{a}^\star_{\mathcal{T}_l(t)} = \arg\min \sum_{t'\in\mathcal{T}_l(t)} c(a_{t'}, s_{t'}, \hat{\omega}_{t'}) \tag{2a}$$

$$\text{s.t. } \forall t' \in \mathcal{T}_l(t),\ s_{t'+\Delta t'} = f(a_{t'}, s_{t'}, \hat{\omega}_{t'}, \Delta t'), \tag{2b}$$

$$s_{t'} \in S'_t, \tag{2c}$$

and applying $a_t^\star$ (potentially changing $a_t^{m,\star}$ at some specific moments only). As forecasts are valid only for a relatively near future and optimizing over a long time horizon would anyway be incompatible with real-time operation, this problem is approximated by cropping the lookahead horizon to $\mathcal{T}_a(t) \subset \mathcal{T}_l(t)$. However, market decisions must be refreshed much less frequently than set-points. We thus propose to further decompose the problem in an operational planning problem (OPP) for $\mathcal{T}_a^m(t)$ that computes market decisions

$$\mathbf{a}^{m,\star}_{\mathcal{T}_a^m(t)} = \arg\min \sum_{t'\in\mathcal{T}_a^m(t)} c^m(a_{t'}^m, s_{t'}, \hat{\omega}_{t'}) \tag{3a}$$

$$\text{s.t. } \forall t' \in \mathcal{T}_a^m(t),\ s_{t'+\Delta\tau} = f^m(a_{t'}^m, s_{t'}, \hat{\omega}_{t'}, \Delta\tau) \tag{3b}$$

$$s_{t'} \in S_{t'}, \tag{3c}$$

and a real-time problem (RTP) that computes set-points for time t

$$a_t^{d,\star} = \arg\min\ c^d(a_t^d, s_t, \hat{\omega}_t) + v_{\tau(t)}(s_{\tau(t)}) \tag{4a}$$

$$\text{s.t. } s_{\tau(t)} = f^d(a_t^d, s_t, \hat{\omega}_t, \tau(t) - t) \tag{4b}$$

$$s_{\tau(t)} \in S_{\tau(t)}, \tag{4c}$$

with $c(a_t, s_t, w_t) = c^m(a_t^m, s_t, w_t) + c^d(a_t^d, s_t, \omega_t)$. The function v_t is the cost-to-go as a function of the state of the system at the end of the ongoing market period, it regularizes decisions of RTP to account for the longer-term evolution of the system. We detail hereunder how we obtain v_t. An overview of the approach is depicted in Figure 1.

[1] Which is here expressed as a deterministic problem for simplicity, but should be treated as a stochastic problem in practice.

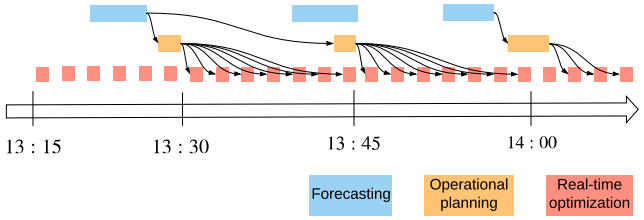

Fig. 1: Hierarchical control procedure illustration.

A. Computing the cost-to-go function $v_{\tau(t)}$

The function v_t represents the optimal value of (3) as a function of the initial state $s_{\tau(t)}$ of this problem. If we make the assumption that (3) is modeled as a linear program, the function $v_{\tau(t)}$ is thus convex and piecewise linear. Every evaluation of (3) with the additional constraint[2]

$$s_{\tau(t)} = s' \perp \mu \tag{5}$$

yields the value $v_{\tau(t)}(s')$ and a supporting inequality (a cut)

$$v_{\tau(t)}(s) \geq v_{\tau(t)}(s') + \mu^T s. \tag{6}$$

The algorithm to approximate $v_{\tau(t)}(s')$ works as follows:

1) estimate the domain of $v_{\tau(t)}$, *i.e.*, the range of states reachable at time $\tau(t)$ and the most probable state that will be reached $s^\star_{\tau(t)}$;
2) evaluate $v_{\tau(t)}(s^\star_{\tau(t)})$ and the associated $\mu^\star$;
3) repeat step 2 for other state values until all regions of $v_{\tau(t)}$ are explored.

Note that if the state is of dimension one and (3) is a linear program, simplex basis validity information can be used to determine for which part of the domain of $v_{\tau(t)}$ the current cut is tight, else a methodology such as proposed in [13] can be used.

B. OPP formulation

The OPP objective function implemented for the case study is

$$J^{OP}_{\mathcal{T}^m_a(t)} = \sum_{t' \in \mathcal{T}^m_a(t)} \left(C^{OP}_{t'} + D^{OP}_{t'} \right) \tag{7}$$

with Operational Planner (OP) the name of this planer. $\mathcal{T}^m_a(t)$ is composed of 96 values with $\Delta_\tau = 15$ minutes and $T_a = 24$ hours. $C^{OP}_{t'}$ models the immediate costs and $D^{OP}_{t'}$ the delayed costs at t'. $C^{OP}_{t'}$ takes into account different revenues and costs related to energy flows: the costs of shed demand, steered and non steered generation, the revenues from selling energy to the grid, the costs of purchasing energy from the grid and the costs for using storage

$$\begin{aligned} C^{OP}_{t'} = \sum_{t' \in \mathcal{T}^m_a(t)} \Bigg(& \sum_{d \in \mathcal{D}^{\text{she}}} \Delta_\tau \pi^{\text{she}}_{d,t'} C^{\text{she}}_{d,t'} a^{\text{she}}_{d,t'} \\ & + \sum_{d \in \mathcal{D}^{\text{ste}}} \Delta_\tau \pi^{\text{ste}}_{d,t'} P^{\text{ste}}_{d,t'} a^{\text{ste}}_{d,t'} \\ & + \sum_{d \in \mathcal{D}^{\text{nst}}} \Delta_\tau \pi^{\text{nst}}_{d,t'} P^{\text{nst}}_{d,t'} a^{\text{nst}}_{d,t'} \\ & + \sum_{d \in \mathcal{D}^{sto}} \Delta_\tau \gamma^{\text{sto}}_d \left(\overline{P}_d \eta^{\text{cha}}_d a^{\text{cha}}_{d,t'} + \frac{\underline{P}_d}{\eta^{\text{dis}}_d} a^{\text{dis}}_{d,t'} \right) \\ & - \pi^{\text{e}}_{t'} e^{\text{gri}}_{t'} + \pi^{\text{i}}_{t'} i^{\text{gri}}_{t'} \Bigg). \end{aligned} \tag{8}$$

$D^{OP}_{t'}$ is composed of the peak cost and symmetric reserve revenue

$$D^{OP}_{t'} = \pi^{\text{p}} \delta p_{t'} - \pi^{\text{s}}_{OP} r^{\text{sym}}_{t'}, \tag{9}$$

$\delta p_{t'}$ is the peak difference between the previous maximum historic peak p_h and the current peak within the market period t'. $r^{\text{sym}}_{t'}$ is the symmetric reserve provided to the grid within the current market period t'.

C. OP constraints

The first set of constraints defines bounds on state and action variables, $\forall t' \in \mathcal{T}^m_a(t)$

$$a^k_{d,t'} \leq 1 \qquad \forall d \in \mathcal{D}^k, \forall k \in \{\text{ste}, \text{she}, \text{nst}\} \tag{10a}$$
$$a^{\text{cha}}_{d,t'} \leq 1 \qquad \forall d \in \mathcal{D}^{sto} \tag{10b}$$
$$a^{\text{dis}}_{d,t'} \leq 1 \qquad \forall d \in \mathcal{D}^{sto} \tag{10c}$$
$$\underline{S}_d \leq s_{d,t'} \leq \overline{S}_d \qquad \forall d \in \mathcal{D}^{sto}. \tag{10d}$$

The energy flows are constrained, $\forall t' \in \mathcal{T}^m_a(t)$, by

$$\begin{aligned} & (e^{\text{gri}}_{t'} - i^{\text{gri}}_{t'})/\Delta_\tau - \sum_{d \in \mathcal{D}^{\text{nst}}} (1 - a^{\text{nst}}) P^{\text{nst}}_{d,t'} + \sum_{d \in \mathcal{D}^{\text{ste}}} a^{\text{ste}}_{d,t'} P^{\text{ste}}_{d,t'} \\ & + \sum_{d \in \mathcal{D}^{\text{nfl}}} C^{\text{nfl}}_{d,t'} + \sum_{d \in \mathcal{D}^{\text{she}}} (1 - a^{\text{she}}_{d,t'}) C^{\text{she}}_{d,t'} \\ & + \sum_{d \in \mathcal{D}^{sto}} \left(\overline{P}_d a^{\text{cha}}_{d,t'} - \underline{P}_d a^{\text{dis}}_{d,t'} \right) = 0 \end{aligned} \tag{11a}$$
$$(e^{\text{gri}}_{t'} - i^{\text{gri}}_{t'})/\Delta_\tau \leq E^{\text{cap}}_{t'} \tag{11b}$$
$$(i^{\text{gri}}_{t'} - e^{\text{gri}}_{t'})/\Delta_\tau \leq I^{\text{cap}}_{t'}. \tag{11c}$$

The dynamics of the state of charge are, $\forall d \in \mathcal{D}^{sto}$

$$s_{d,1} - \Delta_\tau \left(\overline{P}_d \eta^{\text{cha}}_d a^{\text{cha}}_{d,1} - \frac{\underline{P}_d}{\eta^{\text{dis}}_d} a^{\text{dis}}_{d,1} \right) = S^{\text{init}}_d \tag{12a}$$
$$s_{d,t'} - s_{d,t'-\Delta_\tau} - \Delta_\tau \left(\overline{P}_d \eta^{\text{cha}}_d a^{\text{cha}}_{d,t'} - \frac{\underline{P}_d}{\eta^{\text{dis}}_d} a^{\text{dis}}_{d,t'} \right) = 0 \quad , \forall t' \in \mathcal{T}^m_a(t) \tag{12b}$$
$$s_{d,\tau(t+T_a)} = S^{\text{end}}_d. \tag{12c}$$

[2]The $\perp \mu$ notation means that μ is the dual variable of the constraint.

The set of constraints related to the peak power $\forall t' \in \mathcal{T}_a^m(t)$

$$(i_{t'}^{\text{gri}} - e_{t'}^{\text{gri}})/\Delta_\tau \leq p_{t'} \tag{13a}$$
$$-\delta p_{t'} \leq 0 \tag{13b}$$
$$-\delta p_{t'} \leq -(p_{t'} - p_h). \tag{13c}$$

The last constraints define symmetric reserve $\forall t' \in \mathcal{T}_a^m(t)$

$$r_{d,t'}^{s+} \leq \frac{(s_{d,t'} - \underline{S}_d)\,\eta_d^{\text{dis}}}{\Delta_\tau} \quad \forall d \in \mathcal{D}^{sto} \tag{14a}$$
$$r_{d,t'}^{s+} \leq \underline{P}_d(1 - a_{d,t'}^{\text{dis}}) \quad \forall d \in \mathcal{D}^{sto} \tag{14b}$$
$$r_{d,t'}^{s-} \leq \frac{(\overline{S}_d - s_{d,t'})}{\eta_d^{\text{cha}}\Delta_\tau} \quad \forall d \in \mathcal{D}^{sto} \tag{14c}$$
$$r_{d,t'}^{s-} \leq \overline{P}_d(1 - a_{d,t'}^{\text{cha}}) \quad \forall d \in \mathcal{D}^{sto} \tag{14d}$$
$$\begin{aligned} r^{\text{sym, OP}} \leq & \sum_{d \in \mathcal{D}^{sto}} r_{d,t'}^{s+} + \sum_{d \in \mathcal{D}^{\text{ste}}} P_{d,t'}^{\text{ste}}(1 - a_{d,t'}^{\text{ste}}) \\ & + \sum_{d \in \mathcal{D}^{\text{nst}}} P_{d,t'}^{\text{nst}}(1 - a^{\text{nst}}) \\ & + \sum_{d \in \mathcal{D}^{\text{she}}} C_{d,t'}^{\text{she}}(1 - a_{d,t'}^{\text{she}}) \end{aligned} \tag{14e}$$
$$\begin{aligned} r^{\text{sym, OP}} \leq & \sum_{d \in \mathcal{D}^{sto}} r_{d,t'}^{s-} + \sum_{d \in \mathcal{D}^{\text{ste}}} P_{d,t'}^{\text{ste}} a_{d,t'}^{\text{ste}} \\ & + \sum_{d \in \mathcal{D}^{\text{nst}}} P_{d,t'}^{\text{nst}} a^{\text{nst}} + \sum_{d \in \mathcal{D}^{\text{she}}} C_{d,t'}^{\text{she}} a_{d,t'}^{\text{she}}. \end{aligned} \tag{14f}$$

D. RTP formulation

The RTP objective function implemented for the case study is

$$J_t^{RTO} = C_t^{RTO} + D_t^{RTO} + v_{\tau(t)}(s_{\tau(t)}) \tag{15}$$

with Real-Time Optimizer (RTO) the name of this controller. C_t^{RTO} models the immediate costs, D_t^{RTO} the delayed costs and $v_{\tau(t)}(s_{\tau(t)})$ the cost-to-go function of the state of the system at time t within a current market period. C_t^{RTO} is the same as $C_{t'}^{OP}$ by replacing t' by t, Δ_τ by Δ_t and considering only one period of time t. D_t^{RTO} is composed of the peak cost and symmetric reserve penalty costs

$$D_t^{RTO} = \pi^{\text{p}} \delta p_{\tau(t-\Delta_\tau),\tau(t)} + s_t^{TSO} \pi_{RTO}^{\text{s}} \Delta r^{\text{sym}}, \tag{16}$$

$\delta p_{\tau(t-\Delta_\tau),\tau(t)}$ is the peak difference between the previous maximum historic peak p_h and the current peak within the market period computed by RTO. The difference with OP relies on its computation as at t the market period is not finished. Thus the peak within this market period is computed by adding the peak from the beginning of the market period to t and the one resulting from the actions taken from t to the end of the market period. Δr^{sym} is the difference between the symmetric reserve computed by OP and the current reserve within the market period computed by RTO. s_t^{TSO} is the reserve activation signal to activate the tertiary symmetric reserve. It is set by the TSO, 0 if activated, else 1. The activation occurs at the beginning of the next market period.

E. RTO constraints

The set of constraints that defines the bounds on state and action variables and the energy flows are the same as the OP (10) and (11) by replacing t' by t, Δ_τ by Δ_t and considering only one period of time t. The next constraint describes the dynamics of the state of charge $\forall d \in \mathcal{D}^{sto}$ and $\forall t \in \mathcal{T}_i(t)$

$$s_{d,\tau(t)} - \Delta_t \left(\overline{P}_d \eta_d^{\text{cha}} a_{d,t}^{\text{cha}} - \frac{\underline{P}_d}{\eta_d^{\text{dis}}} a_{d,t}^{\text{dis}} \right) = S_{d,t}^{\text{init}}. \tag{17}$$

The set of constraints related to the peak power $\forall t \in \mathcal{T}_i(t)$

$$(i_t^{\text{gri}} - e_t^{\text{gri}})/\Delta_t \leq p_{t,\tau(t)} \tag{18a}$$
$$-\delta p_{\tau(t)} \leq 0 \tag{18b}$$
$$-\delta p_{\tau(t)} \leq -(p_{\tau(t-\Delta_\tau),\tau(t)} - p_h) \tag{18c}$$
$$p_{\tau(t-\Delta_\tau),\tau(t)} = \beta p_{\tau(t-\Delta_\tau),t} + (1-\beta) p_{t,\tau(t)} \tag{18d}$$

with $\beta = 1 - \Delta_t/\Delta_\tau$. The last set of constraints defining the symmetric reserve are the same as the OP (14) by replacing t' by t, $r^{\text{sym, OP}}$ by $r^{\text{sym, RTO}}$ and adding $\forall t \in \mathcal{T}_i(t)$

$$-\Delta r^{\text{sym}} \leq 0 \tag{19a}$$
$$-\Delta r^{\text{sym}} \leq -(r^{\text{sym, OP}} - r^{\text{sym, RTO}}). \tag{19b}$$

IV. Test Description

Our case study is based on the MiRIS microgrid located at the John Cockerill Group's international headquarters in Seraing, Belgium[3]. It is composed of PV, several energy storage devices, and a non-sheddable load. The load and PV data we use come from on-site monitoring. All data, including the weather forecasts, are available on the Kaggle platform[4]. The case study consists of comparing RTO-OP to a Rule-Based Controller (RBC) for three configurations of the installed PV capacity, cf. Table I. The RBC prioritizes the use of PV production for the supply of the electrical demand. If the microgrid is facing a long position, it charges the battery. And if this one is fully charged it exports to the main grid. If the microgrid is facing a short position it prioritizes the use of the battery to supply the demand. And if this one is fully discharged it imports from the main grid. This controller does not take into account any future information, *e.g.*, PV, consumption forecasts, energy prices, or market information such as the peak of the symmetric reserve. Case 3 is the result of a sizing study that defined the optimal device sizes given the PV and consumption data. The sizing methodology used is described in [14].

Figure 2 shows the PV & consumption data over the simulation period: from $May\ 20, 2019$ to $June\ 16, 2019$. The selling price π^{e} is constant, the purchasing price is composed of a day π_d^{i} and night prices π_n^{i}. Day prices apply from 5 a.m. to 8 p.m. (UTC) during the weekdays and night prices apply from 8 p.m. to 5 a.m. during weekdays and the entire weekend. The peak mechanism is taken into account with a constant peak price π^{p} and an initial maximum historic peak

[3] https://johncockerill.com/fr/energy/stockage-denergie/
[4] https://www.kaggle.com/jonathandumas/liege-microgrid-open-data

TABLE I: Case studies parameters and data statistics.

Case	PV_p	$\overline{PV}$	PV_{max}	PV_{min}	PV_{std}
1	400	61	256	0	72
2	875	133	561	0	157
3	1750	267	1122	0	314
Case	C_p	$\overline{C}$	C_{max}	C_{min}	C_{std}
1 - 3	1000	153	390	68	72
Case	S_p	$\overline{S}$, $\underline{S}$	$\underline{P}$, $\overline{P}$	η^{cha}, η^{dis}	S^{init}
1 - 3	1350	1350, 0	1350, 1350	0.95, 0.95	100
Case	p_h, π^p	I^{cap}	E^{cap}	π^i_d, π^i_n	π^e
1 - 3	150, 40	1500	1500	0.2, 0.12	0.035

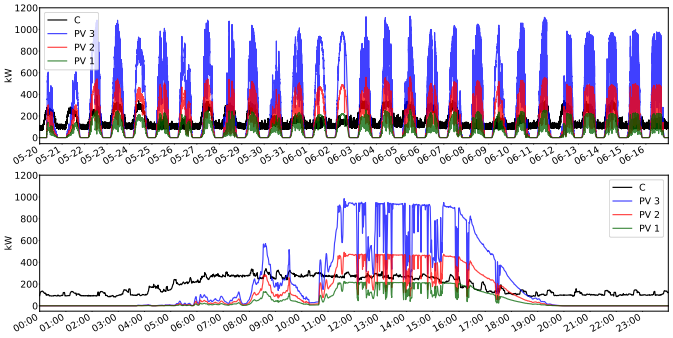

Fig. 2: Top: PV & consumption simulation data. Bottom: zoom on $June\ 12, 2019$.

TABLE II: Results without symmetric reserve.

Case 1	c_E	c_p	c_t	Δ_p	I_{tot}	E_{tot}
RBC	10.13	6.68	16.81	167	61	0
RTO-OP^{RNN}	10.37	3.62	13.99	91	64	1
RTO-OP^{GBR}	10.25	5.27	15.53	132	63	1
RTO-OP*	10.24	0.99	11.23	25	64	1
Case 2	c_E	c_p	c_t	Δ_p	I_{tot}	E_{tot}
RBC	3.19	4.85	8.04	121	22	7
RTO-OP^{RNN}	4.78	2.87	7.65	72	31	15
RTO-OP^{GBR}	4.30	4.90	9.2	123	28	13
RTO-OP*	4.06	0	4.06	0	26	10
Case 3	c_E	c_p	c_t	Δ_p	I_{tot}	E_{tot}
RBC	-2.13	4.12	1.99	105	3	77
RTO-OP^{RNN}	-1.66	4.12	2.46	105	7	80
RTO-OP^{GBR}	-1.67	4.23	2.56	106	7	81
RTO-OP*	-1.90	0	0	0	5	79

p_h. Storage systems are initially fully charged. The PV and consumption data have a 1-second resolution, meaning the RTO could compute its optimization problem each five to ten seconds in operational mode. CPLEX 12.9 is used to solve all the optimization problems, on an Intel Core i7-8700 3.20 GHz based computer with 12 threads and 32 GB of RAM. The average computation time per optimization problem composed of the OP and RTO is a few seconds. However, to maintain a reasonable simulation time RTO is called every minute. The dataset is composed of 28 days with an average computation time of two hours to solve 1440 optimization problems per day, with one-minute resolution, leading to a total of two days for the entire dataset. The OP computes a planning quarterly corresponding to the Belgian market period. The computation time of the RTO on a regular computer is around a few seconds and the OP around twenty seconds. In total, the simulation computation time is up to a few hours. The OP computes quarterly planning based on PV and consumption twenty-four ahead forecasts. The weather-based forecast methodology is described in detail in Annex IX. Two "classic" deterministic techniques are implemented, a Recurrent Neural Network (RNN) with the Keras Python library [15] and a Gradient Boosting Regression (GBR) with the Scikit-learn Python library [16]. These models use as input the weather forecasts provided by the Laboratory of Climatology of the Liège University, based on the MAR regional climate model [12]. It is an atmosphere model designed for meteorological and climatic research, used for a wide range of applications, from km-scale process studies to continental-scale multi-decade simulations. To estimate the impact of the PV and consumption forecast errors on the controllers, the simulation is performed with the OP having access to the PV and consumption future values (RTO-OP*). Then, the simulation is performed with the symmetric reserve mechanisms to cope with the forecast errors. A constant symmetric reserve price π^s_{OP} for the OP and a penalty reserve π^s_{RTO} for the RTO are set to 20 (€/kW).

V. Numerical results

A. No symmetric reserve

Table II provides the simulation results without taking into account the symmetric reserve. The smaller the PV installed capacity the higher the peak and energy costs. The RTO-OP* provides the minimal peak cost whereas the RBC provides the minimal energy cost on all cases. However, RTO-OP* achieves the minimal total cost, composed of the energy and peak costs. This simulation illustrates the impact of the forecasts on the RTO-OP behavior. The RNN forecaster provides the best results but the RTO-OP^{RNN} is still a long way to manage the peak as RTO-OP* due to the forecasting errors. The peak cost strongly penalizes the benefits as it applies on all the year ahead once it has been reached.

In case 3, all the controllers except RTO-OP* reached the maximum peak on $June\ 12, 2019$ around 10:30 a.m. as shown on Figure 4. Figure 2 shows a sudden drop in the PV production around 10 a.m. that is not accurately forecasted by the RNN and GBR forecasters as shown in Figure 3. This prediction leads to a non accurate planning of OP. Thus, the RTO cannot anticipate this drop and has to import at the last minute energy to balance the microgrid. Figure 5 shows

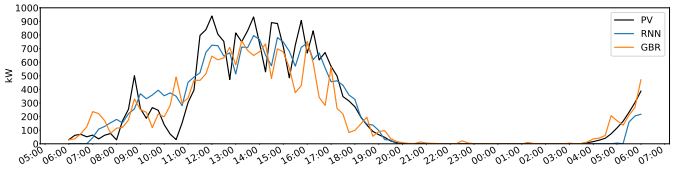

Fig. 3: Case 3 PV forecast on $June\ 12, 2019$, 06h00 UTC.

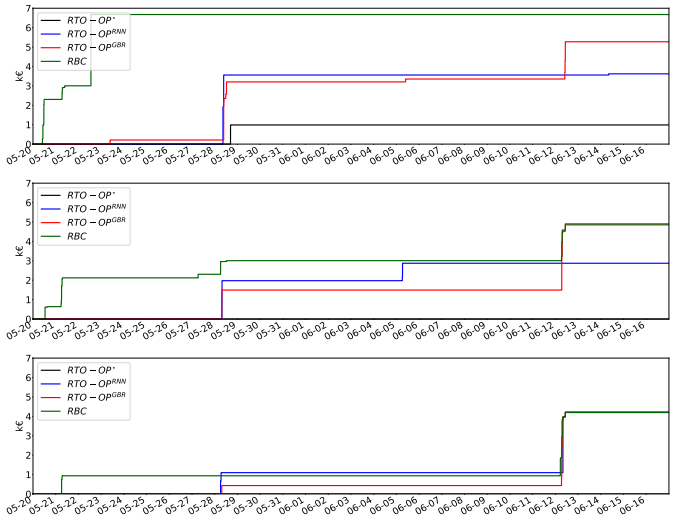

Fig. 4: Case 1 (top), 2 (middle), 3 (bottom) cumulative peak costs.

the controllers behavior on $June\ 12, 2019$ where the peak is reached. In case 2 all controllers reached the same peak as in case 3 except RTO-OP^{RNN} that reached a smaller one on $June\ 5, 2019$. The forecasts accuracy explains this behavior as in case 3. Finally in case 1, each controller reached a different peak. The smallest one is achieved by the RTO-OP*, followed by the RTO-OP^{RNN}. These cases show that the RTO-OP controller optimizes PV-storage usage, and thus requires less installed PV capacity for a given demand level. This result was expected as the peak management is not achieved by the RBC and becomes critical when the PV production is smaller

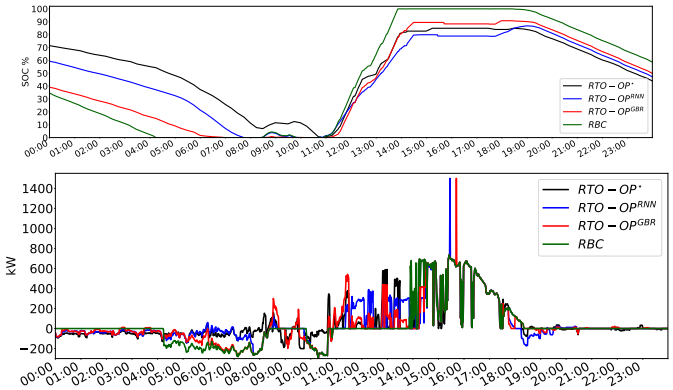

Fig. 5: Case 3 SOC (top) and net export power (bottom) on $June\ 12, 2019$.

TABLE III: Results with symmetric reserve.

Case 1	c_E	c_p	c_t	Δ_p	I_{tot}	E_{tot}
RTO-OP^{RNN}	10.50	2.12	12.62	53	65	3
RTO-OP*	10.47	2.75	13.22	69	65	2
Case 2	c_E	c_p	c_t	Δ_p	I_{tot}	E_{tot}
RTO-OP^{RNN}	5.33	0.04	5.37	1	41	27
RTO-OP*	4.78	0.99	5.77	25	35	20
Case 3	c_E	c_p	c_t	Δ_p	I_{tot}	E_{tot}
RTO-OP^{RNN}	-0.04	0	-0.04	0	24	99
RTO-OP*	-0.15	0	-0.15	0	23.2	98

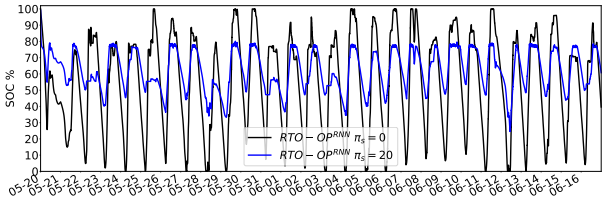

Fig. 6: Case 3 SOC comparison for RTO-OP^{RNN} with and without symmetric reserve.

than the consumption. This simulation also demonstrates the forecast accuracy impact on the RTO-OP behavior.

B. Results with symmetric reserve

Table III provides the simulation results by taking into account the symmetric reserve. Figure 6 depicts on case 3 the behavior differences between RTO-OP^{RNN} without and with symmetric reserve. Figures 7 and 8 show the SOC and peaks costs evolution of case 2 & 1. The controller tends to maintain a storage level that allows RTO-OP^{RNN} to better cope with forecast error. Indeed for case 3, there is no more peak reached by RTO-OP^{RNN}, only 1 kW for case 2 and it has been almost divided by two for case 1. However, this behavior tends to increase the energy cost if the PV production is important in comparison with the consumption, such as in case 3. Indeed, the controller will tend to store more energy in the battery instead of exporting it. RTO-OP* did not perform better with the symmetric reserve. The symmetric reserve competes with the peak management and the RTO-OP* tends to not discharge completely the battery even if it is required to avoid a peak. In case 2, the peak is reached on $June\ 12, 2019$ around 08:00. The controller could have avoided it by totally discharging the battery but did not maintain the reserve level. This is the same behavior in case 1 where the peak could have been limited if all the battery was discharged. There is an economic trade-off to reach to manage the peak and the reserve simultaneously depending on the valorization or not on the market of the symmetric reserve. The reserve can also be valorized internally to cope with non or difficult forecastable events such as a sudden drop of the export or import limits due to loss of equipment or grid congestion.

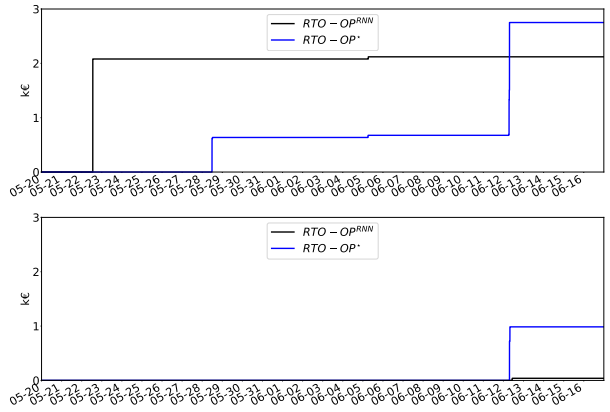

Fig. 7: Case 1 (top) and 2 (bottom) cumulative peak costs.

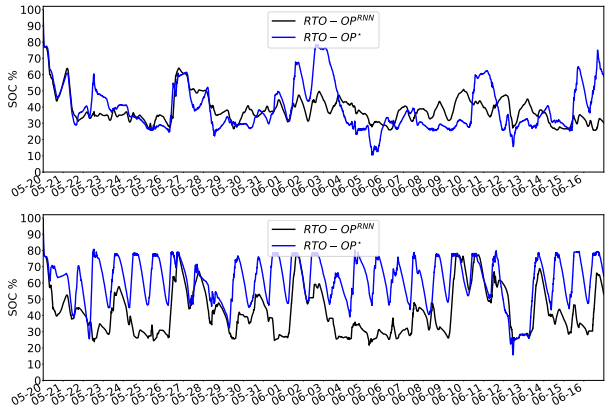

Fig. 8: Case 1 (top) and 2 (bottom) SOC.

VI. Conclusion

A two-level value function-based approach was introduced as a solution method for a multi-resolution microgrid optimization problem. The value function computed by the operational planner based on PV and consumption forecasts allows coping with the forecasting uncertainties. The real-time controller solves an entire optimization problem including the future information propagated by the value function. This approach has been tested on the MiRIS microgrid case study with PV and consumption data monitored on-site. The results demonstrate the efficiency of this method to manage the peak in comparison with a Rule-Based Controller. This test case is completely reproducible as all the data used are open, PV, consumption monitored and forecasted including the weather forecasts. The proposed approach can be extended in several ways. The deterministic formulation of the operational planning problem could be extended to a stochastic formulation, to cope with probabilistic forecasts. Balancing market mechanisms could be introduced. Finally, the approach could be extended to a community by considering several entities inside the microgrid.

VII. Acknowledgment

The authors would like to thank John Cockerill and Nethys for their financial support, and Xavier Fettweis of the Laboratory of Climatology of ULiège who produced the weather forecasts based on the MAR regional climate model.

References

[1] O. Palizban, K. Kauhaniemi, and J. M. Guerrero, "Microgrids in active network management part i: Hierarchical control, energy storage, virtual power plants, and market participation," *Renewable and Sustainable Energy Reviews*, vol. 36, pp. 428–439, 2014.

[2] D. E. Olivares, A. Mehrizi-Sani, A. H. Etemadi, C. A. Cañizares, R. Iravani, M. Kazerani, A. H. Hajimiragha, O. Gomis-Bellmunt, M. Saeedifard, R. Palma-Behnke *et al.*, "Trends in microgrid control," *IEEE Transactions on smart grid*, vol. 5, no. 4, pp. 1905–1919, 2014.

[3] Q. Jiang, M. Xue, and G. Geng, "Energy management of microgrid in grid-connected and stand-alone modes," *IEEE transactions on power systems*, vol. 28, no. 3, pp. 3380–3389, 2013.

[4] X. Wu, X. Wang, and C. Qu, "A hierarchical framework for generation scheduling of microgrids," *IEEE Transactions on Power Delivery*, vol. 29, no. 6, pp. 2448–2457, 2014.

[5] J. Sachs and O. Sawodny, "A two-stage model predictive control strategy for economic diesel-pv-battery island microgrid operation in rural areas," *IEEE Transactions on Sustainable Energy*, vol. 7, no. 3, pp. 903–913, 2016.

[6] S. R. Cominesi, M. Farina, L. Giulioni, B. Picasso, and R. Scattolini, "A two-layer stochastic model predictive control scheme for microgrids," *IEEE Transactions on Control Systems Technology*, vol. 26, no. 1, pp. 1–13, 2017.

[7] C. Ju, P. Wang, L. Goel, and Y. Xu, "A two-layer energy management system for microgrids with hybrid energy storage considering degradation costs," *IEEE Transactions on Smart Grid*, vol. 9, no. 6, pp. 6047–6057, 2017.

[8] B. V. Solanki, C. A. Cañizares, and K. Bhattacharya, "Practical energy management systems for isolated microgrids," *IEEE Transactions on Smart Grid*, 2018.

[9] S. Polimeni, L. Moretti, G. Manzolini, S. Leva, L. Meraldi, and P. Raboni, "Numerical and experimental testing of predictive EMS algorithms for PV-BESS residential microgrid," *IEEE-PES Powertech (accepted)*, p. 6, 2019.

[10] L. Moretti, S. Polimeni, L. Meraldi, P. Raboni, S. Leva, and G. Manzolini, "Assessing the impact of a two-layer predictive dispatch algorithm on design and operation of off-grid hybrid microgrids," *Renewable Energy*, vol. 143, pp. 1439–1453, 2019.

[11] R. Kumar, M. J. Wenzel, M. J. Ellis, M. N. ElBsat, K. H. Drees, and V. M. Zavala, "A stochastic dual dynamic programming framework for multiscale mpc," *IFAC-PapersOnLine*, vol. 51, no. 20, pp. 493–498, 2018.

[12] X. Fettweis, J. Box, C. Agosta, C. Amory, C. Kittel, C. Lang, D. van As, H. Machguth, and H. Gallée, "Reconstructions of the 1900–2015 greenland ice sheet surface mass balance using the regional climate MAR model," *Cryosphere (The)*, vol. 11, pp. 1015–1033, 2017.

[13] A. Bemporad, A. Garulli, S. Paoletti, and A. Vicino, "A greedy approach to identification of piecewise affine models," in *International Workshop on Hybrid Systems: Computation and Control*. Springer, 2003, pp. 97–112.

[14] S. Dakir and B. Cornélusse, "Combining optimization and simulation for microgrid sizing," *Submitted to the 21st Power Systems Computation Conference (PSCC 2020)*, 2019.

[15] F. Chollet *et al.*, "Keras," https://keras.io, 2015.

[16] F. Pedregosa, G. Varoquaux, A. Gramfort, V. Michel, B. Thirion, O. Grisel, M. Blondel, P. Prettenhofer, R. Weiss, V. Dubourg, J. Vanderplas, A. Passos, D. Cournapeau, M. Brucher, M. Perrot, and E. Duchesnay, "Scikit-learn: Machine learning in Python," *Journal of Machine Learning Research*, vol. 12, pp. 2825–2830, 2011.

[17] S. B. Taieb, G. Bontempi, A. F. Atiya, and A. Sorjamaa, "A review and comparison of strategies for multi-step ahead time series forecasting based on the nn5 forecasting competition," *Expert systems with applications*, vol. 39, no. 8, pp. 7067–7083, 2012.

VIII. Notation

Set and indices

- d index of a device
- t, t' indexes of a RTO and OP time periods
- $\tau(t)$ beginning of the next market period at time t
- $\mathcal{T}_i(t) = \{t, t + \Delta t, ..., t + T_i\}$ set of RTO time periods
- $\mathcal{T}_a^m(t) = \{\tau(t), \tau(t) + \Delta\tau, ..., \tau(t + T_a)\}$ set of OP time periods
- T_a, T_l time durations, with $T_a \ll T_l$
- $\mathcal{D}^k$ set of non-flexible loads ($k = $ nfl), sheddable loads ($k = $ she), steerable generators ($k = $ ste), non-steerable generators ($k = $ nst), storage devices ($k = $ sto)

Parameters

- Δ_t time delta between t and the market period (minutes)
- Δ_τ market period (minutes)
- H_T forecasting horizon (hours)
- $\hat{\omega}$ forecast of a random vector ω
- η^{cha}, η^{dis} charge and discharge efficiencies (%)
- $\overline{P}$, $\underline{P}$ maximum charging and discharging powers (kW)
- $C_{d,t}^{\text{nfl}}$ non-flexible power consumption (kW)
- $C_{d,t}^{\text{she}}$ flexible power consumption (kW)
- $S_{d,t}^{\text{init}}$ initial state of charge of battery d (kWh)
- p_h maximum peak over the last twelve months (kW)
- π^{p} yearly peak power cost (€/kW)
- π_{OP}^{s} unitary revenue for providing reserve (€/kW)
- π_{RTO}^{s} unitary RTO symmetric reserve penalty (€/kW)
- $\pi_{d,t}^k$ cost of load shedding ($k = $ she), generating energy ($k = $ ste), curtailing generation ($k = $ nst) (€/kWh)
- $\gamma_{d,t}^{\text{sto}}$ fee to use the battery d (€/kWh)
- π_t^{e}, π_t^{i} energy prices of export and import (€/kWh)
- π_d^{i}, π_n^{i} energy prices of day and night imports (€/kWh)
- I^{cap}, E^{cap} maximum import and export limits (kW)
- PV_p, C_p PV and consumption capacities (kW)
- S_p storage capacity (kWh)
- $\overline{S}$, $\underline{S}$ maximum and minimum battery capacities (kWh)

Forecasted or computed variables

- a_t action at t
- a_t^m purely market related actions
- a_t^d set-points to the devices of the microgrid
- $a_{d,t}^k$ fraction of load shed ($k = $ she), generation activated ($k = $ ste), generation curtailed ($k = $ nst) ($[0, 1]$)
- $a_{d,t}^{\text{cha}}$, $a_{d,t}^{\text{dis}}$ fraction of the maximum charging and discharging powers used for battery d ($[0, 1]$)
- e_t^{gri}, i_t^{gri} energy export and import (kWh)
- $\delta p_{t'}$ OP peak difference between peak at t' and p_h (kW)
- $\delta p_{\tau(t-\Delta_\tau),\tau(t)}$ RTO peak difference between peak at $\tau(t)$ and p_h (kW)
- s_t^{TSO} TSO symmetric reserve signal $(0; 1)$
- r^{sym} symmetric reserve (kW)
- Δr^{sym} reserve difference between OP and RTO (kW)
- $r_{d,t'}^{s+}$, $r_{d,t'}^{s-}$ upward and downward reserves of power available and provided by storage device d (kW)
- $s_{d,t}$ state of charge of battery d (kWh)
- s_t microgrid state at time t
- s_t^m information related to the current market position
- s_t^d state of the devices
- v_t the cost-to-go function
- $\hat{\omega}$ forecast of a random vector ω
- $\overline{\text{X}}$ average of a variable X (kW)
- X_{max}, X_{min} maximum and minimum of X (kW)
- X_{std} standard deviation of X (kW)
- c_E, c_p, c_t energy, peak and total costs (k€)
- Δ_p peak increment (kW)
- I_{tot}, E_{tot} total import and export (MWh)

IX. Annex: forecasting methodology

The inputs of the forecasting method are historical and external data, a forecasting horizon H_T, a resolution, and a forecast frequency. The outputs are the PV production and the consumption. In this study, the input data are weather forecasts and past PV production and consumption series. The horizon is the time range of the forecasts from a few hours to several hours or days. The resolution is the time discretization of the forecast from a few minutes to several hours. The forecast frequency indicates the periodicity at which the forecasts are computed. For instance, a forecasting module with $H_T = 24$ hours, a resolution and periodicity of 15 minutes, computes each quarter, a quarterly forecast for the twenty-four hours ahead. This paper focuses on the real-time control of microgrids based on planning that requires a forecast horizon of a few hours up to a few days.

Two "classic" deterministic techniques are implemented, a Recurrent Neural Network (RNN) with the Keras Python library [15] and a Gradient Boosting Regression (GBR) with the Scikit-learn Python library [16]. The RNN is a Long Short Term Memory (LSTM) with one hidden layer composed of $2 \times n + 1$ neurons with n the number of input features. Both techniques are implemented with a Multi-Input Multi-Output (MIMO) approach [17]. The MIMO strategy consists of learning only one model, $\widehat{m}$, as follows

$$[\widehat{w}^{\tau_1}, ..., \widehat{w}^{\tau_{H_T}}] = \widehat{m}\left[w^{\tau_0}, ..., w^{\tau_{-4}}, \widehat{w}_i^{\tau_1}, ..., \widehat{w}_i^{\tau_{H_T}}\right]. \quad (20)$$

With $\widehat{w}$ the variable to forecast (PV, consumption, etc), $\widehat{w}_i$ the forecast of the i^{th} weather variable such as direct solar irradiance, wind speed, air ambient temperature, etc. The forecast is computed each quarter and composed of $H_T/\Delta\tau$ values $[\widehat{y}^{\tau_1}, ..., \widehat{y}^{\tau_{H_T}}]$. In our case study, $H_T/\Delta_\tau = 96$ with H_T = 24 h and Δ_τ = 15 minutes. The forecasting process is implemented as a rolling forecast methodology. The Learning Set (LS) is refreshed every six hours. The LS is limited to the week preceding the forecasts, to maintain a reasonable computation time.

The forecasts are evaluated using three deterministic metrics: the Normalized Mean Absolute Error (NMAE), the Normalized Root Mean Squared Error (NRMSE), and the Normalized Energy Measurement Error (NEME). The NEME is an NMAE of the energy summed over the entire forecasting horizon. The mean scores $NMAE_{H_T}$, $NRMSE_{H_T}$ and

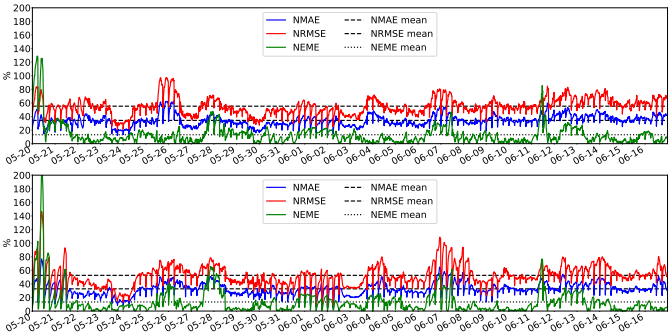

Fig. 9: PV forecast scores for GBR (top) and RNN (bottom).

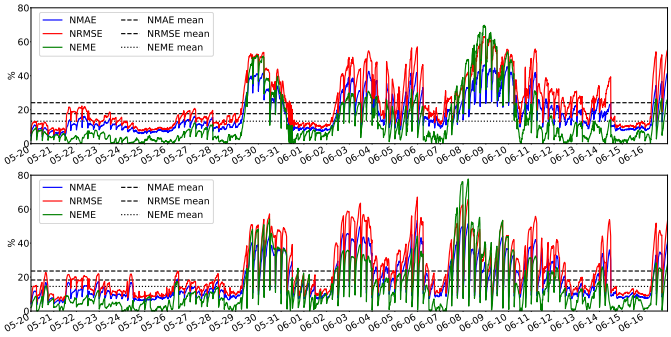

Fig. 10: Consumption forecast scores for GBR (top) and RNN (bottom).

$NEME_{H_T}$ for a forecasting horizon H_T are computed over the entire simulation data set. The normalizing coefficient for computing the NMAE and the NRMSE is the mean of the absolute value of the PV and consumption over all the simulation data set. Figures 9 and 10 provide the scores for both GBR and RNN techniques computed for each quarter of the simulation data set.